

Running title: Glycolysis promotes gastric cancer progression via PI3K/AKT

High glycolysis phenotype influences malignant progression and poor prognosis of gastric cancer through the PI3K/AKT pathway

Shiya Liu^{1,#}, Gaigai Shen^{1,#}, Xuanyu Zhou², Guanghui Wang³, Huiqi Liu³, Yuanting Cao¹, Lixin Sun^{1,*}, Xiong Shu^{4,*}, Yuliang Ran^{1,*}

¹State Key Laboratory of Molecular Oncology, National Cancer Center/National Clinical Research Center for Cancer/Cancer Hospital, Chinese Academy of Medical Sciences and Peking Union Medical College, Chaoyang, Beijing, China; ²Department of Epidemiology and Population Health, Stanford University of Medicine, Stanford, California, United States; ³Department of Basic Medical Sciences, Medical College of Qinghai University, Xining, Qinghai, China; ⁴Beijing Research Institute of Orthopaedics and Traumatology, Beijing Jishuitan Hospital, Capital Medical University, Xicheng, Beijing, China

*Correspondence: sunlixin1x@aliyun.com; shuxiong@jst-hosp.com.cn; ranyuliang@cicams.ac.cn

[#]Contributed equally to this work.

Received March 21, 2025 / Accepted July 10, 2025

Gastric cancer (GC) is a prevalent gastrointestinal malignancy, with metabolic reprogramming, particularly glycolysis, playing a critical role in cancer cell stemness. However, the interaction between glycolysis and GC prognosis, along with its underlying mechanisms, remains poorly understood. This study aimed to systematically analyze the prognostic significance of glycolysis in GC and explore its functional impact. A glycolysis-related gene score was constructed using bioinformatics to assess glycolysis levels based on differentially expressed genes between GC and normal tissues. A nomogram model was developed to predict clinical prognosis, and the functional phenotypes of GC cell lines cultured under high and low glucose conditions were evaluated using metabolite detection and extracellular acidification rate (ECAR) measurements. Enrichment analyses identified key signaling pathways, which were further validated by western blot. Results showed that elevated glycolysis was associated with larger tumor size and poorer prognosis in GC patients. The nomogram demonstrated strong predictive accuracy. High glucose culture promoted glucose consumption, lactate production, ATP generation, and ECAR, enhancing epithelial-mesenchymal transition and malignant progression via the PI3K/AKT pathway. In conclusion, high glycolysis is linked to poor prognosis in GC and drives metastasis and stemness through the PI3K/AKT signaling pathway, highlighting its potential as a prognostic marker and therapeutic target.

Key words: gastric cancer; glycolysis; prognostic; hyperglycemia; PI3K/AKT

45
46
47 Gastric cancer (GC) is the fifth most common malignancy and the fourth leading cause of
48 cancer-related mortality [1, 2]. Despite the decreased global incidence of GC [3], it remains highest
49 in East Asian countries, including China [4]. The efficacy of traditional clinical treatments for GC,
50 including surgery and chemoradiotherapy, is limited, resulting in poor patient prognoses and
51 stagnant five-year survival rates. The primary reasons for the limited efficacy include the complex
52 GC driver genes, high intra-tumor and inter-tumor heterogeneity, and the presence of cancer stem
53 cells (CSCs). CSCs, in particular, contribute to metastasis, recurrence, and drug resistance [5].
54 Metabolism plays a crucial role in GC and impacts patient prognosis [6]. Epithelial-mesenchymal
55 transition (EMT) represents a reversible cellular program that may serve as a pivotal early stage of
56 tumor metastasis [7]. Furthermore, hyperglycemia promotes cell invasion and metastasis in various
57 cancers [8]. However, the mechanisms underlying this phenomenon remain unclear.

58 Metabolic reprogramming, an emerging hallmark of cancer [9], has gained substantial attention in
59 the last few years. The relationship between metabolic reprogramming and cancer has been
60 extensively validated, and glycolysis is a crucial pathway for energy metabolism reprogramming in
61 tumor cells. Tumor cells exhibit significantly elevated glycolysis levels, preferentially utilizing this
62 pathway for energy production under both hypoxic and aerobic environments [10]. Metabolic
63 reprogramming has been observed in vivo in various tumor types and is closely associated with the
64 maintenance of CSCs, cancer progression, metastasis, and drug resistance [11]. Metabolism,
65 particularly glycolysis, is intricately linked with EMT and stemness in tumor cells [12, 13].
66 Alterations in glycolysis levels in tumor cells are associated with stemness-associated
67 characteristics exhibited by the entire tumor cell population [14]. Under normal circumstances,
68 cells are not affected by any changes in intracellular glucose metabolism due to changes in blood
69 sugar in the body. However, tumor cells are highly sensitive to fluctuations in glucose concentration
70 in the external environment, thereby regulating intracellular glucose metabolism and changing their
71 metabolic mode to ensure survival and further metastasis and proliferation. However, the regulation
72 of glycolysis in tumor cells and its role in controlling EMT and metastasis remain unclear.

73 Consequently, we investigated the effects of elevated glucose levels on EMT and stemness in
74 tumors. In this study, the effects of high glucose levels on GC cell metastasis and stemness were
75 evaluated using both clinical data and biological experiments. Furthermore, the objective of this

study was to gain preliminary insight into the molecular mechanisms through which high glucose exerts these effects. Our results have significant clinical implications for identifying specific targets and inhibitors related to tumor metabolism and stemness [11]. Thus, our findings provide valuable insights into GC that may contribute to developing new therapeutic strategies.

Materials and methods

Cell lines and culture. The human GC cell lines MGC803 and HGC27 were obtained from the Chinese Academy of Sciences (China). The cells were cultured in DMEM complete media containing 10% fetal bovine serum, 1% L-glutamine, penicillin, and streptomycin. All cells were cultured in a 37 °C incubator with 5% CO₂.

Data processing and establishment of the GRG score model. Gene expression data were extracted from The Cancer Genome Atlas (TCGA) database. The "limma" package was used to select differentially expressed genes (DEGs) between the tumor and normal tissues with the following criteria: FDR-adjusted p-values < 0.05 and |fold change| > 1.5. The Molecular Signatures Database (MSigDB) v4.0 was searched for glycolysis-related gene sets (HALLMARK_GLYCOLYSIS). Gene set enrichment analysis (GSEA) was performed on DEGs to identify pathways and networks potentially involved in GC progression. From the 4266 DEGs, 54 GRGs were identified using a Venn diagram. Next, Cox regression analysis and Least Absolute Shrinkage and Selection Operator (LASSO) regression were performed to identify glycolytic target genes associated with overall survival (OS) to establish GRG score model. The GRG scores for patients with stomach adenocarcinoma (STAD) were calculated based on the coefficients (Coefi) and expression levels (Expri) of the prospective prognostic GRGs using the following formula:

$$\text{GRG score} = \sum_{i=1}^n \text{Coefi} \times \text{Expri}.$$

Construction and evaluation of the GRG prognostic model. Data from the TCGA database were used as the training set. The median GRG score (median=0.033) was used as the cutoff to divide 355 TCGA-STAD patients into high and low glycolysis groups. Kaplan-Meier curves were plotted to compare the OS between the high and low GRG score groups. Time-dependent receiver operating characteristic (ROC) curves were used to evaluate the predictive ability of the GRG score model. To validate the prognostic model, the same process was carried out on a testing dataset from the Gene Expression Omnibus (GEO) (GSE62254, N=300).

106 **Development of a nomogram based on GRG scores and clinical factors in TCGA-STAD.** The
107 "compare Groups" R package was used to compare the predictive efficacy of the GRG score with
108 clinical characteristics. Cox regression analysis was applied to evaluate the independent prognostic
109 value of the GRG scores and other clinical features. A nomogram was constructed using the R
110 package "rms" and "regplot" to predict prognosis, based on GRG scores and clinical features.
111 Calibration plots of the nomograms were created to assess the predictive accuracy of the nomogram
112 using the "caret" package. ROC curves were used to validate the predictive ability of the
113 nomogram.

114 **GRG score model differential analysis and enrichment analysis.** The TCGA-STAD dataset was
115 divided into 2 groups based on the median glycolysis score. DEGs were selected using the
116 following criteria: FDR-adjusted p-values < 0.05 and |fold change| > 1.5 between the high and low
117 GRG score group. The differential biological effects and signaling pathways between the high and
118 low glycolysis groups in the gene ontology (GO) and Kyoto Encyclopedia of Genes and Genomes
119 (KEGG) databases were evaluated using the "cluster Profiler" package in R. GSEA was employed
120 to assess whether expression of specific gene sets from the MSigDB collection
121 (hall.v2023.1.Hs.symbols.gmt) were significantly different between the high and low glycolysis
122 groups.

123 **Calculation of EMT and stemness scores.** The pan-cancer 78-gene EMT signature was
124 downloaded from the EMTome online database (<https://www.emtome.org/>) [15]. The expression
125 levels of the 78 genes were calculated as the sum across all samples. The top 10 mesenchymal
126 genes (MGene_top10) and the top 10 epithelial genes (EGene_top10) were defined. The EMT score
127 for each sample (panCancer_EMTscore) was calculated as the difference in expression values
128 between the MGene_top10 and EGene_top10. A higher EMT score indicates a more mesenchymal
129 phenotype and a less epithelial phenotype. The stemness score (ssGSVA score) was constructed
130 with the "GSVA" R package using 109 cancer stem cell-related genes compiled from previous
131 research [16].

132 **Glucose consumption and lactate production measurement.** Cells were seeded into 6-well plates.
133 After 24 h, 2 ml of fresh medium was used instead. Following a fixed incubation period, the cell
134 culture supernatant was collected. Glucose consumption was assessed using a colorimetric method
135 according to the instructions of the Glucose and Sucrose Assay Kit (Sigma-Aldrich, #MAK013,

136 USA). Lactate production was measured using the Lactate Assay Kit II (Abcam, #ab65331, UK).
137 Glucose consumption and lactate production were normalized to the number of cells ($\mu\text{mol}/10^6$
138 cells).

139 **Adenosine 5'-triphosphate (ATP) production measurement.** Cells were seeded into 6-well plates.
140 After 24 h, 2 ml of fresh medium was used instead. Following a fixed incubation period, the cells
141 were collected, and ATP production was measured using the ATP Assay Kit (Beyotime, #S0027,
142 China). ATP production was normalized to the control group (nmol/mg protein).

143 **Extracellular acidification rate (ECAR) measurement.** Cells were seeded in XF96 plates (15,000
144 cells/well) and incubated overnight. After washing, the cells were incubated in a 37 °C CO₂-free
145 incubator for 60 min. Glucose (10 mM), oligomycin (1 μM), and 2-deoxyglucose (2-DG, 50 mM)
146 were added, and ECAR was measured at the specified time points. The ECAR was assessed using
147 the Seahorse XFe96 analyzer (Agilent Technologies Inc., USA) to evaluate glycolytic flux.

148 **Oxygen consumption rate (OCR) measurement.** Cells were seeded in XF96 plates (15,000
149 cells/well) and incubated overnight. After washing, the cells were incubated in a 37 °C CO₂-free
150 incubator for 60 min. Oligomycin (1 μM), Carbonyl cyanide 4-(trifluoromethoxy) phenylhydrazone
151 (FCCP, 1 μM), and rotenone/antimycin A (0.5 μM) were sequentially added, and OCR was
152 measured at the specified time points. OCR was determined using the Seahorse XFe96 analyzer
153 (Agilent Technologies Inc., USA) to assess mitochondrial respiration.

154 **Cell invasion and migration assay.** To assess cell migration and invasion, Transwell™ chambers
155 (24-well inserts; pore size, 8 μm ; Corning, USA) were either left uncoated or coated with diluted
156 Matrigel (BD Biosciences, USA). Serum-starved cells (2×10^4) were seeded in the upper chamber
157 with serum-free medium, while the lower chamber contained complete medium with varying
158 glucose concentrations. After 24 h of incubation at 37 °C, the cells that had migrated through the
159 membrane were fixed, stained, photographed, and counted. Quantitative analysis was then
160 performed to assess cell migration and invasion.

161 **Cell proliferation analysis.** Cells cultured in high- and low-glucose environments were seeded in
162 96-well plates (approximately 5,000 cells/well) and cultured in media with different glucose
163 concentrations. Using the IncuCyte S3 platform (Sartorius, Göttingen, Germany), phase contrast
164 images were collected from two regions within each well at 3 h intervals using a 10× objective. The
165 IncuCyte S3 image analysis software was set to detect cell edges and determine their confluence

percentage. Proliferation curves were plotted based on the confluence percentage over time to evaluate cell proliferation capacity.

Sphere formation assay. A solution of 0.8% methylcellulose was prepared [14], and 2 ml of the solution was added to each well of a low-adhesion 24-well plate. Cells were cultured in high- and low-glucose environments during their logarithmic growth phase and harvested. The cell density was adjusted to 5×10^4 cells/ml and 10 μ l of the cell suspension was added to the methylcellulose in each well. Cells were incubated at 37 °C with 5% CO₂ for 7-14 days. Photograph and count the number and size of spheres under an inverted fluorescence microscope.

Colony formation assay. Cells are cultured in high- and low-glucose environments during their logarithmic growth phase. The cell density was adjusted to 5×10^3 cells/ml and 20 μ l of the cell suspension was added to each well of a 6-well plate and gently shaken to disperse the cells. Every 3 days, 1 ml of the corresponding fresh medium was added. Cells were incubated at 37 °C until visible colonies formed. The colonies were fixed with 2 ml of 4% formaldehyde (Solarbio, China) for 30 min, stained with 2 ml of 0.1% crystal violet (Solarbio, China) for 30 min, rinsed with PBS, air dried, and photographed. Count the number of colonies formed in each group.

Protein extraction and western blot. Cells cultured in high- and low-glucose environments were lysed to extract total protein. The proteins were separated using SDS-PAGE and transferred to membranes, followed by the addition of ECL detection reagent for visualization. Western blot band grayscale values were quantified using ImageJ software. Target protein band densities were normalized to the corresponding β -actin internal control.

The following primary antibodies were used: CD44 (#ab157107), SOX2 (#ab97959), and Oct4 (#ab18976), were from Abcam (USA), and vimentin (#5741S), β -actin (#4970S), E-cadherin (#3195S), N-cadherin (#13116S), Snail (#3879S), Nanog (#3580S), p-PI3K (#4228S), PI3K (#4249S), p-AKT (#4060S) and AKT (#2920S) were from Cell Signaling Technology (USA). Secondary antibodies were HRP-labeled goat anti-rabbit and anti-mouse IgG (Jackson, USA).

Statistical analysis. Statistical analysis and data visualization were performed using R version 4.2.0, SPSS 25.0, and GraphPad Prism 8.0. All experiments were repeated three times, and the data are presented as means \pm standard deviation ($\bar{x} \pm s$). Normality and homogeneity of variance analyses were conducted on the data. $P < 0.05$ was considered statistically significant.

196 Results

197 **Impact of the high glycolysis model on prognosis in patients with GC.** Using TCGA data, we
198 identified DEGs between GC and normal tissues (Supplementary Figure S1A). Based on the
199 glycolysis gene set from the hallmark database, glycolysis genes were significantly enriched in GC
200 patients (Supplementary Figure S1B). After integrating DEGs from TCGA, we selected 54
201 glycolysis-related DEGs in tumor tissues versus normal tissues for further study (Supplementary
202 Figure S1C). After filtering through LASSO and multivariable Cox regression analysis
203 (Supplementary Figures S1D, S1E), 4 genes (STC1, VCAN, SOX9, and AK4) significantly
204 associated with OS were identified ($p < 0.05$). GRG scores were calculated using the following
205 formula: $\text{GRG score} = (0.1908 \times \text{STC1}) + (0.1034 \times \text{VCAN}) + (-0.1660 \times \text{SOX9}) + (0.1216 \times \text{AK4})$.
206 STAD patients were divided into high and low glycolysis groups based on the GRG scores. The
207 heatmap displays the expression profiles of the four genes. Compared to the low glycolysis group,
208 the expression levels of AK4, STC1, and VCAN were higher in the high glycolysis group, whereas
209 SOX9 expression was lower in the high glycolysis group (Figure 1A).

210 The relationship between the survival status and time of GC patients was ranked by GRG scores
211 (Figure 1B). Based on the Kaplan-Meier survival analysis, the predictive model exhibited strong
212 prognostic capability, with the low glycolysis group showing a higher survival rate and patients in
213 the high glycolysis group showing shorter survival times ($p < 0.005$; Figure 1C). The predictive
214 ability of the prognostic model was validated using the 1-year, 3-year, and 5-year ROC curves; the
215 AUC values of the ROC curves were all above 0.6, indicating that the GRG score model accurately
216 predicted prognosis in patients with GC (Figure 1D).

217 The ACGR cohort (GSE62254, N=300) from the GEO database was selected as the testing gene set
218 to verify the GRG scoring model using the same methodology. The distribution of the four
219 GRG-related genes in the heatmap plot (Figure 1E) and the survival status stratified by median
220 GRG scores (median=0.411; Figure 1F) were similar to the previous findings. The Kaplan-Meier
221 survival curves demonstrated that the survival rate of the low glycolysis group was higher than the
222 survival rate of the high glycolysis group (Figure 1G), consistent with the results from the
223 TCGA-STAD. Additionally, the GRG score-based model exhibited good sensitivity and specificity,
224 with AUC values above 0.6 in ROC curves (Figure 1H). Further analysis of the relationship
225 between the GRG score and clinical pathological characteristics revealed that high glycolysis levels

were associated with larger tumor size in patients with GC (Supplementary Table S1, Supplementary Figure S2A). Meanwhile, the TCGA project has classified gastric cancer into four molecular subtypes including genome stable (GS), MSI, EBV, and chromosomal instability (CIN). We found that the distribution of GRGscore varies significantly among different molecular subtypes and higher GRG score cases were concentrated on the subtypes of GS (Supplementary Figures S2B, S2C).

Nomogram for predicting prognosis in GC patients combining glycolysis and clinical characteristics. A glycolysis-clinical nomogram was developed to predict individual survival rates based on glycolysis and clinical factors. First, Cox regression analyses were conducted to evaluate the GRG score and other clinical features. The univariate Cox results indicated that age, stage, Tumor node metastasis (TNM) classification, and the GRG score, were associated with OS (Figure 2A). More total points were associated with shorter 1-year, 3-year, and 5-year survival times (Figure 2B). Multivariate regression revealed only 3 independent prognostic factors (Supplementary Table S1). Calibration curves comparing the predicted survival times with observed 1-year, 3-year, and 5-year survival times (Figure 2C) indicated that the nomogram prediction model accurately predicted the survival time of patients with GC within a 5-year period.

The GRG score model exhibited better predictive accuracy compared to clinical features such as tumor grade and TNM classification. The nomogram model combining the GRG score with significant clinical features from the multivariate Cox analysis exhibited the highest AUC (> 0.7) (Figure 2D). Thus, combining glycolysis and clinical factors reliably predicted patient prognosis, highlighting the clinical significance of glycolysis.

High and low glucose culture environments induce different glycolytic phenotypes in GC cells.

To verify the impact of glycolysis on the malignant GC phenotype, MGC803 and HGC27 GC cell lines were cultured in media with 25 mM, 15 mM, and 5.5 mM glucose to establish cell lines with varying glycolytic phenotypes. Treatment with different glucose concentrations significantly altered the glycolytic levels in GC cells. A high-glucose environment significantly increased glucose consumption and the production of major glycolytic products, including lactate and ATP (Figures 3A-3C). High-glucose culture also significantly elevated the ECAR levels in GC cells (Figure 3D). Conversely, a low-glucose environment significantly reduced glucose consumption, lactate production, ATP generation, and ECAR in GC cells. We further performed mitochondrial oxygen

consumption rate (OCR) assays in MGC803 and HGC27 cells. The results demonstrated that neither basal respiration, maximal respiratory capacity, nor ATP-linked respiration showed significant alterations under different glucose concentrations (5.5 mM, 15 mM, and 25 mM) (Supplementary Figure S3). These results indicate that high glucose environment induces a high-glycolytic phenotype and low glucose environment induces a low-glycolytic phenotype in GC cells. Thus, these culture conditions were used for subsequent cell models.

High-glucose environment promotes malignant phenotypes in GC cells. Changes in the functional phenotypes of GC cells in high- and low-glucose culture environments were determined. The proliferation rates of GC cells cultured in a high-glucose environment were significantly higher than the proliferation rates of cells cultured in a low-glucose environment (Figure 4A). Colony formation assays demonstrated that the number of colonies formed increased with higher glucose concentrations (Supplementary Figure S4A). Thus, increased glycolysis significantly enhances the proliferative capacity of GC cells. The numbers of migrating and invading cells were significantly higher in the high-glucose culture group compared with the numbers in the low-glucose culture group, indicating that the migration and invasion abilities of GC cells increased under high-glucose conditions (Figure 4B, Supplementary Figure S4B). Sphere formation assays indicated that the number of spheres formed by GC cells significantly increased in cells cultured in high-glucose concentrations compared with the number of spheres in cells cultured in low-glucose conditions, indicating that the stem cell-like properties of GC cells were enhanced in a high-glucose environment (Figure 4C). Overall, these results demonstrate that increased glycolysis levels are associated with the malignant phenotype of GC cells, including metastasis and stemness, and a high-glucose environment promotes these malignant traits.

High-glucose environment promotes GC progression via the PI3K/AKT pathway. To further investigate the mechanisms by which high glucose regulates GC progression, DEGs in GC patients with high and low glycolysis in the TCGA-STAD dataset were analyzed. 2248 genes were upregulated and 165 genes were downregulated in the high glycolysis group compared to the low glycolysis group (Figure 5A). DEGs were mainly enriched in biological functions such as extracellular matrix, cell adhesion, and migration, according to GO analysis (Supplementary Figure S5A). And KEGG analysis demonstrated that DEGs were mainly enriched in the PI3K/AKT pathway (Figure 5B). GSEA analysis further confirmed that the PI3K/AKT (Figure 5C) was

286 significantly enriched in GC with high glycolysis. This was further validated by western blot
287 analysis (Figure 5D, Supplementary Figure S6A), which demonstrated increased activation of the
288 PI3K/AKT in GC cells with increasing glucose concentrations in the culture environment.
289 Collectively, these results suggest that high glycolysis in GC enhances malignant phenotypes such
290 as metastasis and stemness by activating the PI3K/AKT signal pathway.

291 **High-glucose environment promotes EMT and stemness in GC.** The GSEA analysis indicated
292 that the EMT and P53 pathways were significantly enriched in the high glycolysis group within the
293 hallmark gene sets (Supplementary Figure S5B). Based on previous findings on the functional
294 phenotypes of GC cells, it is tenable to hypothesize that a high-glucose environment influences
295 EMT and stemness in GC. The EMTome database [15] was utilized to download a pan-cancer
296 78-gene EMT signature, which was employed to construct an EMT score. EMT scores were
297 significantly elevated in the high glycolysis group compared with the EMT scores in the low
298 glycolysis group (Figure 6A), and EMT scores significantly correlated with GRG scores (Figure
299 6B). Expression levels of EMT-related markers (N-cadherin, vimentin, and snail) were significantly
300 higher in GC cells cultured in a high-glucose environment compared with cells cultured in a
301 low-glucose environment (Figure 6C, Supplementary Figure S6B), confirming that increased
302 glycolysis promotes EMT in GC cells.

303 A stemness score was constructed using 109 tumor stem cell genes, as previously described [16].
304 Stemness scores were significantly elevated in the high glycolysis group compared to the scores in
305 the low glycolysis group (Figure 6D); GRG scores significantly correlated with stemness (Figure
306 6E). WB analysis confirmed the stemness-related molecular phenotype in GC cells. The expression
307 levels of stemness-related markers (CD44, OCT4, and SOX2) were significantly higher in GC cells
308 cultured in a high-glucose environment compared with the expression levels in GC cells cultured in
309 a low-glucose environment (Figure 6F, Supplementary Figure S6C). Thus, elevated glycolysis
310 influences stemness in GC cells.

311

312 **Discussion**

313 Despite recent advances in the diagnosis and treatment of GC, drug resistance is associated with
314 low survival rates. Thus, identifying novel therapeutic targets and strategies for patients with GC is
315 urgently needed [17]. High blood glucose levels are associated with poorer prognoses in cancer

316 patients, including those with GC [18, 19]. Diabetes is known to increase the risk of various cancers,
317 such as liver, pancreatic, colorectal, and GCs. Most cancer patients with uncontrolled plasma
318 glucose levels have poorer prognoses and shorter survival times [20, 21]. This highlights the impact
319 of glucose metabolism on tumor stemness and metastasis [22, 23].

320 Increasing evidence suggests that relying on single clinical factors or individual gene characteristics
321 often results in poor predictive performance. Now, we can focus on identifying a series of the most
322 critical genes related to patient survival predictions, rather than conducting broad explorations. We
323 constructed a high glycolysis score model (GRG score) based on clinical data and demonstrated that
324 high glucose levels affect the prognosis of patients with GC, consistent with previous research
325 findings [22, 23]. Subsequent survival analysis revealed that patients in the high GRG score group
326 had worse prognoses. This result was validated with an independent ACGA cohort. The distribution
327 of GRG scores differed significantly across molecular subtypes, with enrichment of high glycolysis
328 in the GS subtype. These findings suggest that metabolic phenotypes may complement genomic
329 classifications and offer an additional layer of tumor stratification, potentially paving the way for
330 refined prognostic and therapeutic frameworks. GRG scores and clinical characteristics were
331 combined into a nomogram. The nomogram is an effective tool for the clinical diagnosis and
332 treatment of GC patients. These results indicate that GRG scores and the nomogram strongly
333 predict the prognosis of patients with GC and can guide clinical treatment decisions [24].

334 Subsequently, a high-glucose state was simulated in vitro by culturing cells in a high-glucose
335 medium, thereby mimicking hyperglycemia. Prolonged exposure to elevated glucose levels
336 increased glycolysis and enhanced malignancy-related phenotypes associated with cancer stemness
337 [18]. The proliferation, migration, invasion, and self-renewal abilities of GC cells were significantly
338 enhanced when exposed to high glucose. Active glycolysis is a hallmark of malignancy, typically
339 accompanied by elevated levels of glycolytic enzymes and corresponding metabolites. Nevertheless,
340 the precise mechanisms by which glycolysis contributes to tumorigenesis are unclear [25].

341 Increasing evidence indicates that metabolism, particularly glycolysis, and cancer stemness are
342 intricately intertwined processes within tumor tissues [26]. Tumor cells exhibit active glycolytic
343 activity and a strong dependence on glycolysis [27]. Abnormal increases in glycolytic intermediates
344 or products are markers of enhanced cancer stemness and chemoresistance [13]. Additionally, CSCs
345 exhibit significantly increased glucose uptake and lactate production and reduced mitochondrial

346 respiration [28]. Leveraging these metabolic changes may provide effective targeted therapeutic
347 strategies, reducing the risk of recurrence and metastasis [29].

348 Regarding the molecular mechanisms of glucose-driven oncogenesis, glucose is widely recognized
349 to promote cancer progression through various metabolic pathways. Tumor cells are capable of
350 sensing extracellular glucose fluctuations and adaptively modulating intracellular metabolic flux,
351 thereby regulating glycolytic activity and influencing stemness-related properties that contribute to
352 tumor initiation and progression. In this study, we evaluated the effects of different glucose
353 concentrations on glycolysis and oxidative phosphorylation (OXPHOS) by measuring ECAR and
354 OCR, respectively. The results demonstrated that OXPHOS activity remained relatively stable
355 across the tested glucose concentrations, whereas glycolytic activity, as indicated by ECAR,
356 exhibited more pronounced dynamic changes in response to extracellular glucose levels.

357 Previous studies have shown that tumor cells display highly dynamic metabolic adaptations to
358 glucose availability, with the magnitude and direction of these shifts largely dependent on tumor
359 type and metabolic plasticity. For instance, in glioblastoma, lower glucose concentrations (100
360 mg/L) are associated with increased OCR, suggesting compensatory reliance on OXPHOS when
361 glycolytic flux is restricted. In contrast, at higher glucose levels (1,000-4,500 mg/l), glycolytic
362 reserve increases while OCR decreases, indicating a metabolic shift toward glycolysis [30].
363 Conversely, in breast cancer cells, glucose deprivation suppresses both ECAR and OCR,
364 accompanied by ATP depletion, lactate reduction, mitochondrial depolarization, and activation of
365 pyroptotic pathways [31]. These findings underscore the significant intertumoral variability in
366 metabolic regulation and OXPHOS dependency.

367 Our findings further support the notion that gastric cancer cells exhibit a distinct form of metabolic
368 flexibility, maintaining relatively stable mitochondrial respiration while dynamically adjusting
369 glycolytic activity in response to extracellular glucose availability. These observations complement
370 the broader understanding that glucose promotes cancer progression through multiple metabolic
371 pathways, including glycolysis, the tricarboxylic acid (TCA) cycle, glycosylation, and lipid
372 synthesis. Such metabolic reprogramming contributes to the activation of oncogenic signaling
373 pathways, enhancing tumor cell proliferation, metastasis, drug resistance, and angiogenesis.
374 Furthermore, high glucose levels can upregulate key enzymes in glucose metabolism, leading to
375 increased glycolysis, glycosylation modifications, lactate production, and lipid synthesis. These

alterations in energy metabolism activate signaling pathways associated with invasive tumor phenotypes [18, 32], promoting tumor cell proliferation, metastasis, drug resistance, and angiogenesis. Hyperglycemia, both directly and indirectly, is associated with an increased risk for carcinogenesis. The mechanisms through which hyperglycemia contributes to carcinogenic pathways are numerous and complex. These include direct or indirect DNA damage, reactive oxygen species (ROS) formation, mutation accumulation, impaired DNA repair, and aberrant regulation of oncogenes and tumor suppressor genes [33]. These metabolic reprogramming and tumor microenvironment modifications ultimately promote cancer development and progression. The p53 checkpoint bypasses independent of mutations may represent the carcinogenic origin and targetable susceptibility of glucose-driven cancers [34]. Additionally, glucose can promote cancer without being metabolized. Glucose functions as an oncogenic signaling molecule that directly binds to NSUN2, inhibiting the activation of the STING pathway. Suppression of the STING pathway impedes the activation and infiltration of antitumor T cells, ultimately promoting cancer initiation and progression [35].

Energy-responsive growth signaling pathways are implicated in metabolic reprogramming to support abnormal proliferation and metastasis [36, 37]. As a key oncogenic signaling pathway, PI3K/AKT has emerged as an important therapeutic target in cancer treatment due to its central role in regulating tumor cell proliferation, survival, metabolism, and resistance. Our results demonstrate the effects of high glucose-mediated glycolysis on PI3K/AKT signaling in GC. This finding validates the impact of glycolysis on EMT and stemness-related biological and molecular phenotypes in tumor cells, consistent with previous studies [38]. Notably, several PI3K inhibitors have already been approved for clinical use in certain cancer types, and multiple PI3K/AKT-targeted agents are currently under active clinical investigation [39, 40]. Meanwhile, it is essential to acknowledge the constraints of our study when interpreting the results. The culturing of GC cells in varying glucose concentrations can only simulate a high-glucose environment and does not accurately represent the in vivo hyperglycemic environment. In addition, the current study is limited by the availability of cell models, and future investigations incorporating low-passage primary gastric cancer cells or patient-derived models would provide more clinically relevant insights. Furthermore, given that our analysis relies solely on retrospective TCGA data, future prospective clinical studies are needed to validate the relationship between blood glucose levels,

therapeutic response, and tumor progression.

In conclusion, we demonstrate that elevated glycolysis is associated with worse clinical prognoses in patients with GC. A predictive model combining glycolysis and clinical features are developed and validated to assess patient prognosis. Additionally, we simulate a high-glucose environment by culturing GC cells in various glucose concentrations. This approach demonstrates that the high-glycolysis phenotype induced by a high-glucose environment significantly impacts malignant characteristics such as metastasis and stemness in GC cells. This mechanism may involve the PI3K/AKT pathway, which promotes EMT and regulates GC stemness by influencing glycolysis levels. Moving forward, we plan to investigate the mechanistic role of PI3K/AKT signaling through pharmacological inhibition and assess the therapeutic potential of combined targeting of glycolysis and the PI3K/AKT pathway. Our findings highlight the necessity for clinical attention to GC patients with hyperglycemia and present novel strategies and therapeutic targets for GC diagnosis and treatment by elucidating the underlying mechanisms.

Acknowledgements: This work was financially supported by National Key Research and Development Program of China (No.2022YFC2409902), National Natural Science Foundation of China (82073278), Beijing Municipal Health Commission (BMHC-2021-6, BJRITO-RDP-2023, XT-2024-06, JYY2023-11, JYY2023-8), CAMS Innovation Fund for Medical Sciences (2021-I2M-1-067), Middle-aged and Young Scientist Fund of Qinghai University Medical College (2023-kyt-2), Xining Science and Technology Bureau People's Livelihood Science and Technology Special Program (2019-M-15), The Independent Issue of State Key Laboratory of Molecular Oncology (SKLMO-2025-17).

References

- [1] THRIFT AP, WENKER TN, EL-SERAG HB. Global burden of gastric cancer: epidemiological trends, risk factors, screening and prevention. *Nat Rev Clin Oncol* 2023; 20: 338-349. <https://doi.org/10.1038/s41571-023-00747-0>
- [2] BRAY F, LAVERSANNE M, SUNG H, FERLAY J, SIEGEL RL et al. Global cancer statistics 2022: GLOBOCAN estimates of incidence and mortality worldwide for 36 cancers in 185 countries. *CA Cancer J Clin* 2024; 74: 229-263. <https://doi.org/10.3322/caac.21834>
- [3] THRIFT AP, EL-SERAG HB. Burden of Gastric Cancer. *Clin Gastroenterol Hepatol*. 2020; 18: 534-542. <https://doi.org/10.1016/j.cgh.2019.07.045>

- 439 [4] TOKUNAGA M, SATO Y, NAKAGAWA M, ABURATANI T, MATSUYAMA T et al.
 440 Perioperative chemotherapy for locally advanced gastric cancer in Japan: current and future
 441 perspectives. *Surg Today* 2020; 50: 30-37. <https://doi.org/10.1007/s00595-019-01896-5>
- 442 [5] LOH JJ, MA S. Hallmarks of cancer stemness. *Cell Stem Cell* 2024; 31: 617-639.
 443 <https://doi.org/10.1016/j.stem.2024.04.004>
- 444 [6] CHEN H, ZHENG X, ZONG X, LI Z, LIN et al. Metabolic syndrome, metabolic comorbid
 445 conditions and risk of early-onset colorectal cancer. *Gut* 2021; 70: 1147-1154.
 446 <https://doi.org/10.1136/gutjnl-2020-321661>
- 447 [7] DONGRE A, WEINBERG RA. New insights into the mechanisms of
 448 epithelial-mesenchymal transition and implications for cancer. *Nat Rev Mol Cell Biol* 2019;
 449 20: 69-84. <https://doi.org/10.1038/s41580-018-0080-4>
- 450 [8] MURPHY N, SONG M, PAPADIMITRIOU N, CARRERAS-TORRES R, LANGENBERG
 451 C et al. Associations Between Glycemic Traits and Colorectal Cancer: A Mendelian
 452 Randomization Analysis. *J Natl Cancer Inst* 2022; 114: 740-752.
 453 <https://doi.org/10.1093/jnci/djac011>
- 454 [9] HANAHAN D, WEINBERG RA. Hallmarks of cancer: the next generation. *Cell* 2011; 144:
 455 646-674. <https://doi.org/10.1016/j.cell.2011.02.013>
- 456 [10] WARBURG O, WIND F, NEGELEIN E. The Metabolism of Tumors in the Body. *J Gen*
 457 *Physiol* 1927; 8: 519-530. <https://doi.org/10.1085/jgp.8.6.519>
- 458 [11] PAPADAKI S, MAGKLARA A. Regulation of Metabolic Plasticity in Cancer Stem Cells
 459 and Implications in Cancer Therapy. *Cancers (Basel)* 2022; 14.
 460 <https://doi.org/10.3390/cancers14235912>
- 461 [12] DI FRANCESCO AM, TOESCA A, CENCIARELLI C, GIORDANO A, GASBARRINI A
 462 et al. Metabolic Modification in Gastrointestinal Cancer Stem Cells: Characteristics and
 463 Therapeutic Approaches. *J Cell Physiol* 2016; 231: 2081-2087.
 464 <https://doi.org/10.1002/jcp.25318>
- 465 [13] CHEN K, ZHANG C, LING S, WEI R, WANG J et al. The metabolic flexibility of quiescent
 466 CSC: implications for chemotherapy resistance. *Cell Death Dis* 2021; 12: 835.
 467 <https://doi.org/10.1038/s41419-021-04116-6>
- 468 [14] YANG T, SHU X, ZHANG HW, SUN LX, YU L et al. Enolase 1 regulates stem cell-like
 469 properties in gastric cancer cells by stimulating glycolysis. *Cell Death Dis* 2020; 11: 870.
 470 <https://doi.org/10.1038/s41419-020-03087-4>
- 471 [15] MAK MP, TONG P, DIAO L, CARDNELL RJ, GIBBONS DL et al. A Patient-Derived,
 472 Pan-Cancer EMT Signature Identifies Global Molecular Alterations and Immune Target
 473 Enrichment Following Epithelial-to-Mesenchymal Transition. *Clin Cancer Res* 2016; 22:
 474 609-620. <https://doi.org/10.1158/1078-0432.CCR-15-0876>
- 475 [16] MIRANDA A, HAMILTON PT, ZHANG AW, PATTNAIK S, BECHT E et al. Cancer
 476 stemness, intratumoral heterogeneity, and immune response across cancers. *Proc Natl Acad*
 477 *Sci U S A* 2019; 116: 9020-9029. <https://doi.org/10.1073/pnas.1818210116>
- 478 [17] MORGAN E, ARNOLD M, CAMARGO MC, GINI A, KUNZMANN AT et al. The current
 479 and future incidence and mortality of gastric cancer in 185 countries, 2020–2034: A
 480 population-based modelling study. *eClinicalMedicine* 2022; 47.
 481 <https://doi.org/10.1016/j.eclinm.2022.101404>

- [18] SUPABPHOL S, SEUBWAI W, WONGKHAM S, SAENGBONMEE C. High glucose: an emerging association between diabetes mellitus and cancer progression. *J Mol Med (Berl)* 2021; 99: 1175-1193. <https://doi.org/10.1007/s00109-021-02096-w>
- [19] HU Y, ZHANG X, MA Y, YUAN C, WANG M et al. Incident Type 2 Diabetes Duration and Cancer Risk: A Prospective Study in Two US Cohorts. *J Natl Cancer Inst* 2021; 113: 381-389. <https://doi.org/10.1093/jnci/djaa141>
- [20] NIK-AHD F, HOWARD LE, EISENBERG AT, ARONSON WJ, TERRIS MK et al. Poorly controlled diabetes increases the risk of metastases and castration-resistant prostate cancer in men undergoing radical prostatectomy: Results from the SEARCH database. *Cancer* 2019; 125: 2861-2867. <https://doi.org/10.1002/cncr.32141>
- [21] ZHENG J, XIE SH, SANTONI G, LAGERGREN J. Population-based cohort study of diabetes mellitus and mortality in gastric adenocarcinoma. *Br J Surg* 2018; 105: 1799-1806. <https://doi.org/10.1002/bjs.10930>
- [22] HE X, CHENG X, DING J, XIONG M, CHEN B et al. Hyperglycemia induces miR-26-5p down-regulation to overexpress PFKFB3 and accelerate epithelial-mesenchymal transition in gastric cancer. *Bioengineered* 2022; 13: 2902-2917. <https://doi.org/10.1080/21655979.2022.2026730>
- [23] XU X, CHEN B, ZHU S, ZHANG J, HE X et al. Hyperglycemia promotes Snail-induced epithelial-mesenchymal transition of gastric cancer via activating ENO1 expression. *Cancer Cell Int* 2019; 19: 344. <https://doi.org/10.1186/s12935-019-1075-8>
- [24] SHEN G, LIU S, CAO Y, CHEN Z, WANG G et al. HSP90 co-regulates the formation and nuclear distribution of the glycolytic output complex to promote resistance and poor prognosis in gastric cancer patients. *J Transl Med* 2025; 23: 172. <https://doi.org/10.1186/s12967-025-06196-w>
- [25] SANCHO P, BARNEDA D, HEESCHEN C. Hallmarks of cancer stem cell metabolism. *Br J Cancer* 2016; 114: 1305-1312. <https://doi.org/10.1038/bjc.2016.152>
- [26] SHEN YA, CHEN CC, CHEN BJ, WU YT, JUAN JR et al. Potential Therapies Targeting Metabolic Pathways in Cancer Stem Cells. *Cells* 2021; 10. <https://doi.org/10.3390/cells10071772>
- [27] PAUL S, GHOSH S, KUMAR S. Tumor glycolysis, an essential sweet tooth of tumor cells. *Sem Cancer Biol* 2022; 86: 1216-1230. <https://doi.org/10.1016/j.semcancer.2022.09.007>
- [28] BRUNGS D, AGHMESHEH M, VINE KL, BECKER TM, CAROLAN MG et al. Gastric cancer stem cells: evidence, potential markers, and clinical implications. *J Gastroenterol* 2016; 51: 313-326. <https://doi.org/10.1007/s00535-015-1125-5>
- [29] KROEMER G, POUYSSEGUR J. Tumor cell metabolism: cancer's Achilles' heel. *Cancer Cell* 2008; 13: 472-482. <https://doi.org/10.1016/j.ccr.2008.05.005>
- [30] MIKI K, YAGI M, YOSHIMOTO K, KANG D, UCHIUMI T. Mitochondrial dysfunction and impaired growth of glioblastoma cell lines caused by antimicrobial agents inducing ferroptosis under glucose starvation. *Oncogenesis* 2022; 11: 59. <https://doi.org/10.1038/s41389-022-00437-z>
- [31] YE J, HU P, ZHANG R, ZHOU L, LUO Z et al. Targeting Hyperglycemic Bone Pre-Metastatic Niche for Breast Cancer Bone Metastasis Therapy. *Adv Sci (Weinh)* 2025; e04924. <https://doi.org/10.1002/advs.202504924>
- [32] LIU S, SHEN G, ZHOU X, SUN L, YU L et al. Hsp90 Promotes Gastric Cancer Cell Metastasis and Stemness by Regulating the Regional Distribution of Glycolysis-Related

Metabolic Enzymes in the Cytoplasm. *Adv Sci (Weinh)* 2024; e2310109. <https://doi.org/10.1002/advs.202310109>

[33] RAMTEKE P, DEB A, SHEPAL V, BHAT MK. Hyperglycemia Associated Metabolic and Molecular Alterations in Cancer Risk, Progression, Treatment, and Mortality. *Cancers (Basel)* 2019; 11. <https://doi.org/10.3390/cancers11091402>

[34] SU Y, LUO Y, ZHANG P, LIN H, PU W et al. Glucose-induced CRL4(COP1)-p53 axis amplifies glycometabolism to drive tumorigenesis. *Mol Cell* 2023; 83: 2316-2331.e2317. <https://doi.org/10.1016/j.molcel.2023.06.010>

[35] CHEN T, XU ZG, LUO J, MANNE RK, WANG Z et al. NSUN2 is a glucose sensor suppressing cGAS/STING to maintain tumorigenesis and immunotherapy resistance. *Cell Metab* 2023; 35: 1782-1798.e1788. <https://doi.org/10.1016/j.cmet.2023.07.009>

[36] SUN Y, ZHANG X, HANG D, LAU HC, DU J et al. Integrative plasma and fecal metabolomics identify functional metabolites in adenoma-colorectal cancer progression and as early diagnostic biomarkers. *Cancer Cell* 2024; 42: 1386-1400.e1388. <https://doi.org/10.1016/j.ccell.2024.07.005>

[37] SEMENTINO E, HASSAN D, BELLACOSA A, TESTA JR. AKT and the Hallmarks of Cancer. *Cancer Res* 2024; 84: 4126-4139. <https://doi.org/10.1158/0008-5472.Can-24-1846>

[38] SHU X, CAO KY, LIU HQ, YU L, SUN LX et al. Alpha-enolase (ENO1), identified as an antigen to monoclonal antibody 12C7, promotes the self-renewal and malignant phenotype of lung cancer stem cells by AMPK/mTOR pathway. *Stem Cell Res Ther* 2021; 12: 119. <https://doi.org/10.1186/s13287-021-02160-9>

[39] FONTANA F, GIANNITTI G, MARCHESI S, LIMONTA P. The PI3K/Akt Pathway and Glucose Metabolism: A Dangerous Liaison in Cancer. *Int J Biol Sci* 2024; 20: 3113-3125. <https://doi.org/10.7150/ijbs.89942>

[40] OCCHIUZZI MA, LICO G, IOELE G, DE LUCAM, GAROFALO A et al. Recent advances in PI3K/PKB/mTOR inhibitors as new anticancer agents. *Eur J Med Chem* 2023; 246: 114971. <https://doi.org/10.1016/j.ejmech.2022.114971>

Figure Legends

Figure 1. Glycolysis-related gene (GRG) score analyses in patients with gastric cancer (GC) in the training and testing sets based on the four-GRGs. A) Heatmap of the four-GRG expression profile. B) Distribution of GRG scores per patient. C) Survival status and survival times of GC patients according to GRG scores. D) Kaplan-Meier plots showing overall survival (OS) in high- and low-GRG score groups. E, F) External validation of the GRG score model using expression data from the ACGA database.

Figure 2. Combining glycolysis and clinical features to construct a nomogram for predicting the prognosis of GC patients. A) Forest plot illustrating the univariate Cox regression of the GRG

566 scores and corresponding clinical features. B) Age, TNM, stage, and GRG score were employed in
567 the Nomogram, and the total score was used to predict the 1-, 3-, and 5-year prognosis of patients
568 with GC. C) Calibration curve of the Nomogram to predict survival within 5 years. D) Receiver
569 operating characteristic curves (ROC) curves for predicting prognosis using different predictive
570 models at 1 year, 3 years, and 5 years.

571

572 **Figure 3.** High and low glucose culture conditions induce high and low glycolytic phenotypes in
573 GC cells. A) Glucose consumption, B) lactate production, C) intracellular adenosine 5'-triphosphate
574 (ATP) production, and D) extracellular acidification rate (ECAR) in MGC803 and HGC27 cells
575 cultured in different glucose concentrations. Data are shown as means±SD. **p < 0.01, ***p <
576 0.001

577

578 **Figure 4.** Culturing in different glucose concentrations affects the stem-related features of GC cells.
579 A) Cell proliferation capacity, B) self-renewal ability (scale bar, 1000 μm), and (C) invasion ability
580 (scale bar, 100 μm) of MGC803 and HGC27 cells cultured in different glucose concentrations. Data
581 are presented as means±SD. *p < 0.05, **p < 0.01, ***p < 0.001.

582

583 **Figure 5.** High-glucose environment culture contributes to the progression of GC via the
584 PI3K/AKT pathway. A) Volcano plot showing the distribution of differentially expressed genes
585 (DEGs) in high and low glycolysis-related gene (GRG) score groups. B) KEGG enrichment
586 analysis of DEGs between the high and low GRG score groups. C) GSEA analysis of PI3K/AKT
587 genes between the high and low GRG score groups. D) Western blots showing phosphorylation of
588 proteins in the PI3K/AKT pathway in GC cells cultured in different glucose concentrations.

589

590 **Figure 6.** High-glucose environment promotes epithelial-mesenchymal transition (EMT) and
591 stemness in GC. A) Violin plot comparing the distribution of the EMT scores in the high- and
592 low-GRG score groups. B) Correlation between the EMT and GRG scores in the TCGA database. C)
593 Western blots showing expression of EMT-related markers in GC cells cultured in different glucose
594 concentrations. D) Violin plot analysis comparing stemness scores in the high- and low-GRG score
595 groups. E) Correlation between stemness and GRG scores in the TCGA database. F) Western blots

596 showing expression of stemness markers in GC cells cultured in different glucose concentrations.

Accepted manuscript

Fig. 1 [Download full resolution image](#)

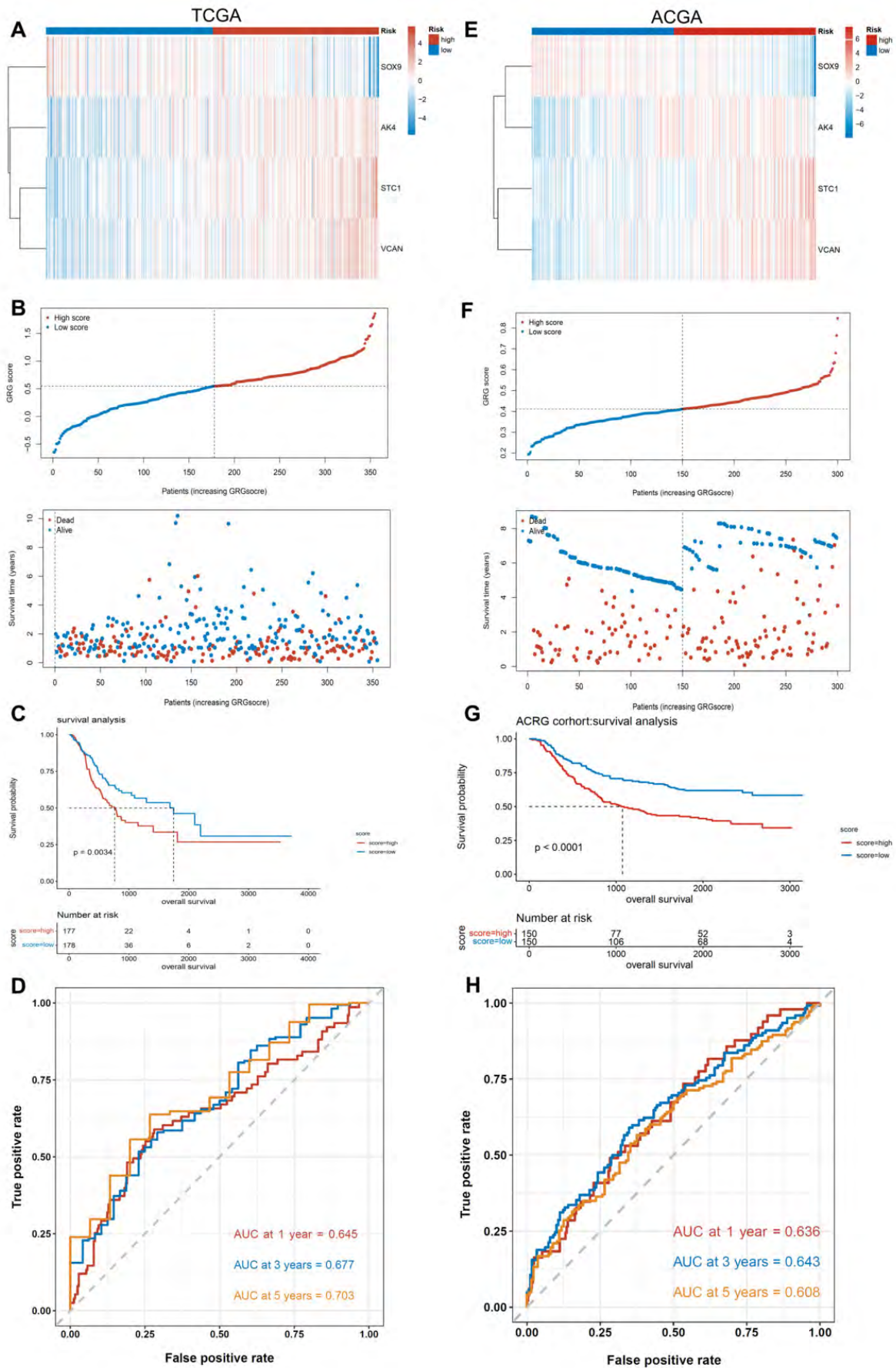


Fig. 2 [Download full resolution image](#)

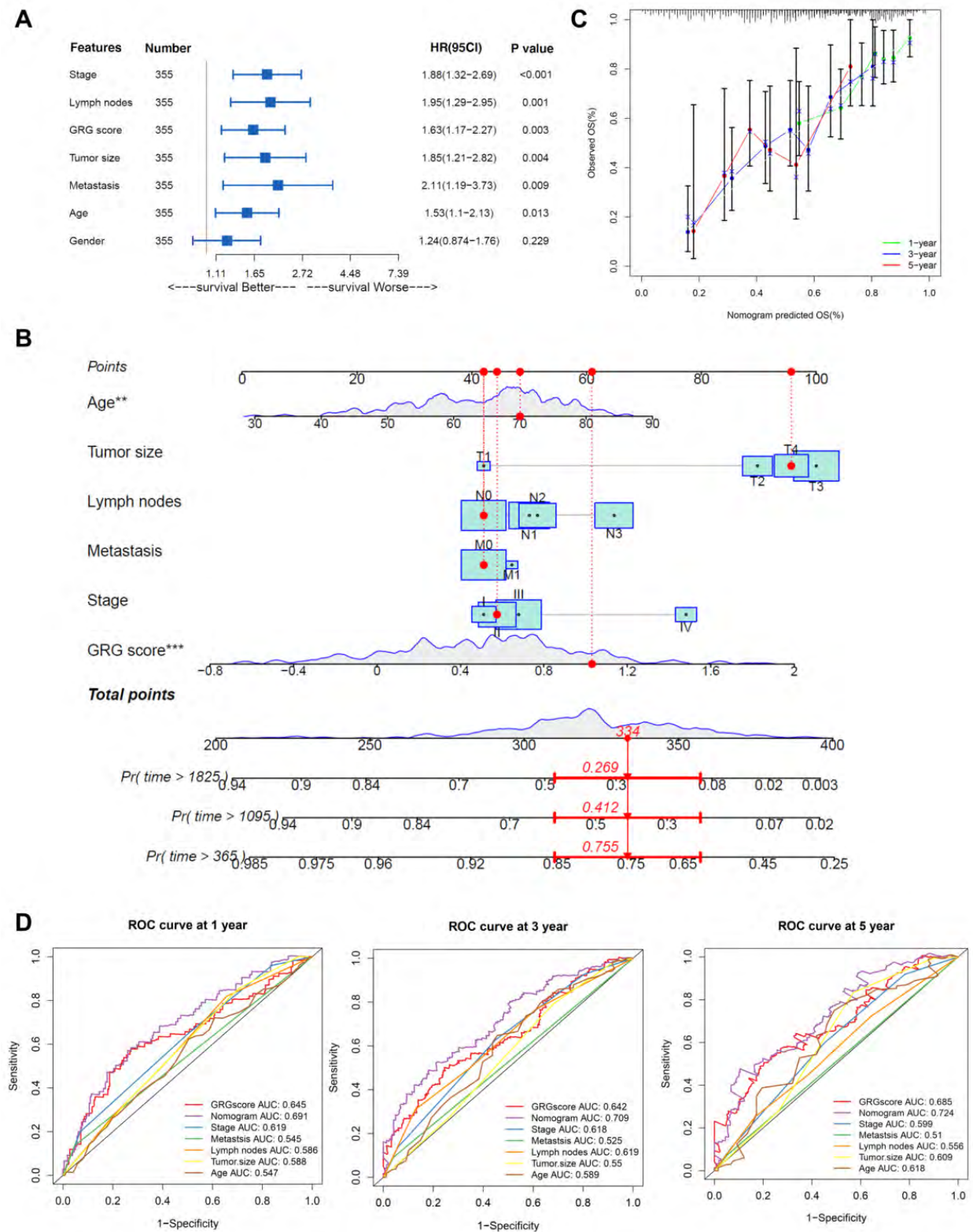


Fig. 3 [Download full resolution image](#)

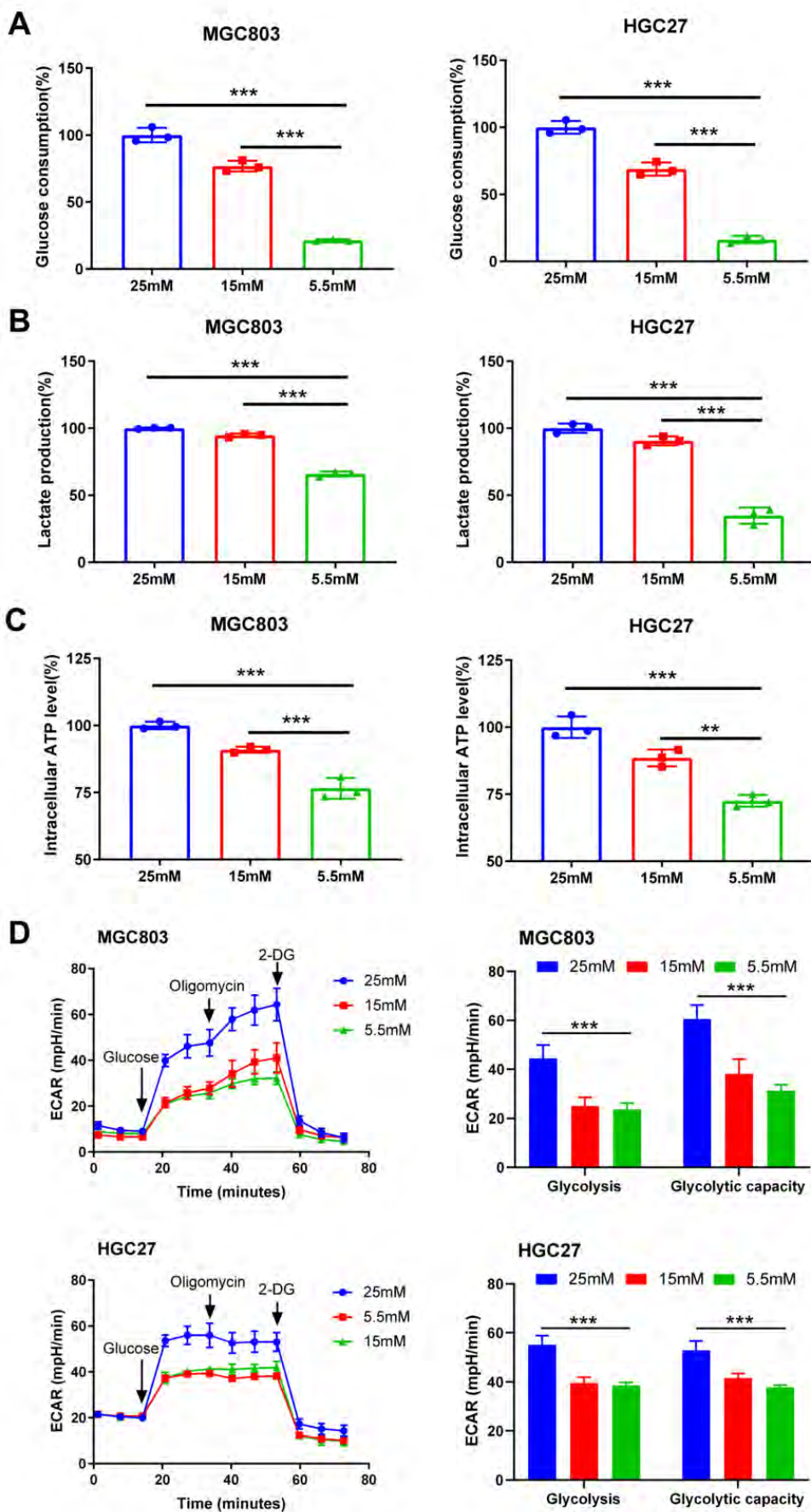


Fig. 4 [Download full resolution image](#)

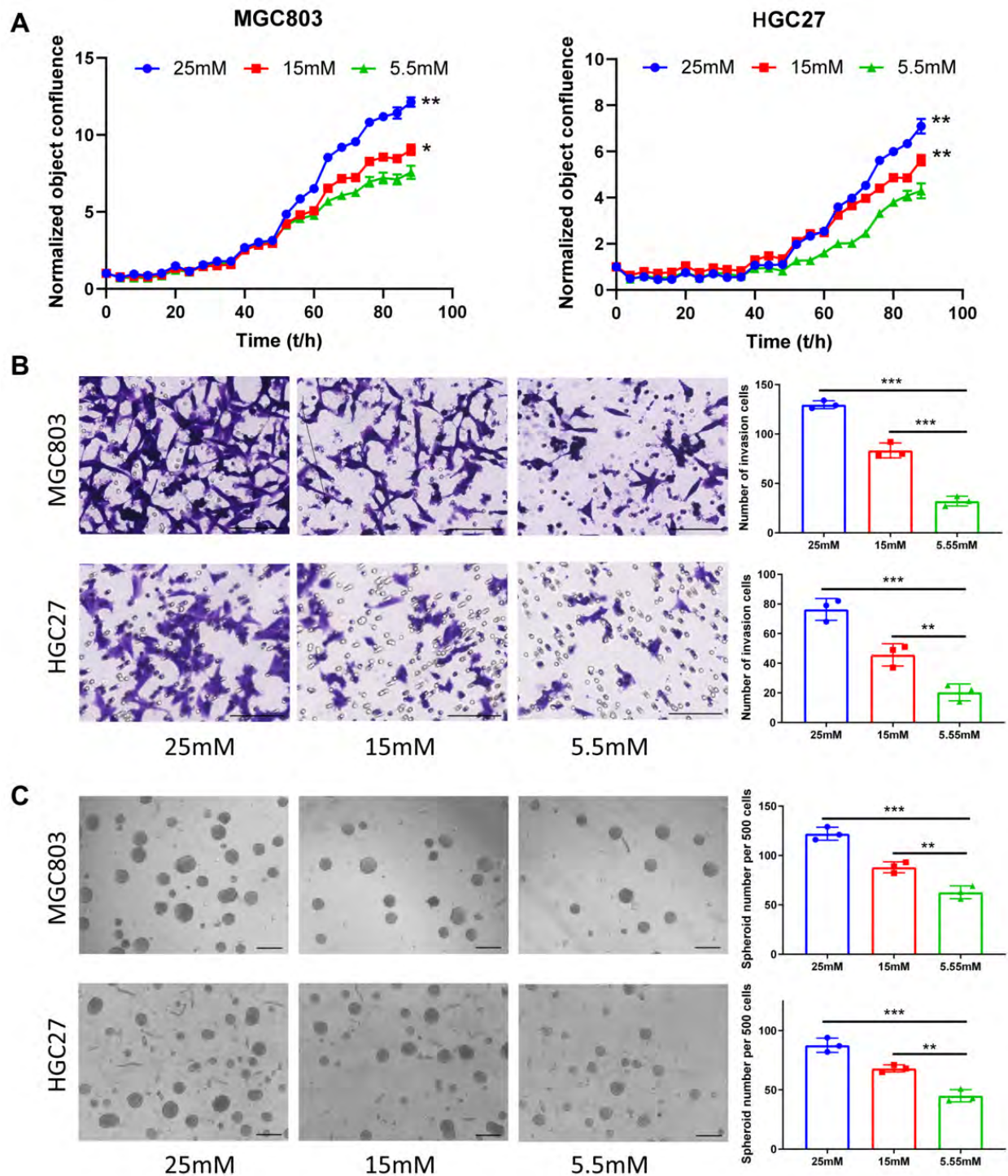


Fig. 5 [Download full resolution image](#)

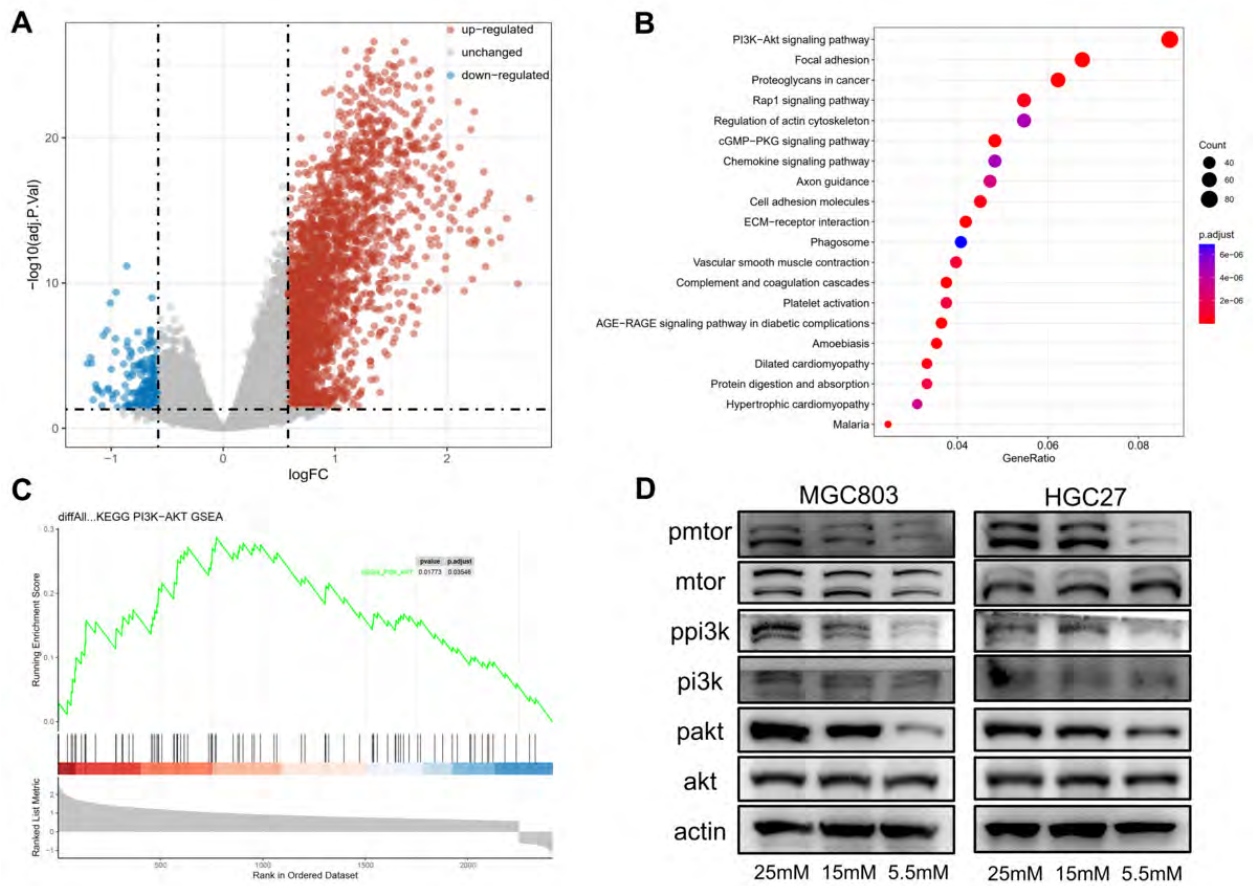


Fig. 6 [Download full resolution image](#)

